Rapid adaptation to elevated extracellular potassium in the pyloric circuit of the crab, *Cancer borealis*

Abbreviated title: Loss and recovery of circuit activity in high [K^+]

Lily S. He*, Mara C.P. Rue*, Ekaterina O. Morozova*, Daniel J. Powell, Eric J. James[+], Manaswini Kar[o], and Eve Marder

Biology Department and Volen Center, Brandeis University, Waltham, MA 02454

[+] Biology Department, Aldephi University, Garden City, NY 11530

[o] Department of Neurobiology, University of Pittsburgh, Pittsburgh, PA 15213

* these authors contributed equally to this work

Corresponding author: Eve Marder: marder@brandeis.edu

Number of pages: 42

Number of figures: 6

Abstract: 223 words

Introduction: 625 words

Discussion: 1484 words

The authors declare no conflicts of interest.

Acknowledgments: Supported by NSF Grant *R35 NS097343*. The authors would like to thank Daniel Shin for assistance with dissections, and Stephen Van Hooser for statistical advice, and Sonal Kedia and Jason Pipkin for careful reading of this manuscript.

Abstract

Elevated extracellular [K^+] is associated with many disorders including epilepsy, traumatic brain injury, ischemia and kidney failure. Experimentally, elevated [K^+] is used to increase excitability in neurons and networks, by shifting the potassium equilibrium potential (E_K) and consequently, the resting membrane potential. We studied the effects of increased extracellular [K^+] on the well-described pyloric circuit of the crab, *Cancer borealis*, while recording pyloric network activity extracellularly and the activity of Pyloric Dilator neuron (PD) intracellularly. A 2.5-fold increase in extracellular [K^+] (2.5x[K^+]) depolarized PD neurons and resulted in an unexpected short-term loss of their normal bursting activity. This period of silence was followed by the recovery of spiking and/or bursting activity during the continued superfusion of 2.5x[K^+] saline. In contrast, when PD neurons were pharmacologically isolated from pyloric presynaptic inputs, they exhibited no loss of spiking activity in 2.5x[K^+], suggesting the existence of an acute inhibitory effect mediated by circuit interactions. Action potential threshold in PD neurons decreased markedly over the course of exposure to 2.5x[K^+] concurrent with the recovery of spiking and/or bursting activity. This study illustrates a case of rapid adaptation to a global perturbation that is influenced by local synaptic connections. Moreover, the complex response of pyloric neurons to elevated [K^+] demonstrates that electrophysiological recordings are necessary to determine how neuronal and circuit activity are affected by altered K^+ concentrations.

Significance Statement

To characterize the sensitivity of a neuronal circuit to global perturbation, we tested the response of the well-described pyloric circuit of the crab stomatogastric ganglion to saline with elevated [K^+]. Unexpectedly, a 2.5-fold increase in extracellular [K^+] led to a temporary loss of activity in pyloric neurons that is not due to depolarization block. This was followed by a rapid increase in excitability and concurrent recovery of spiking activity within minutes. In contrast, when presynaptic inputs to pyloric neurons were blocked, there was no temporary loss of spiking activity in elevated [K^+]. This is a case of rapid adaptation that restores neuronal activity disrupted by global depolarization.

Introduction

Neuronal circuits must be robust to various environmental challenges. This is especially true for central pattern generators (CPGs) that produce essential motor patterns such as breathing, walking, and chewing (Marder and Calabrese, 1996). Maintaining stability over a range of perturbations involves multiple intrinsic and synaptic mechanisms that operate across minutes to days (Von Euler, 1983; Marder and Bucher, 2001; Harris-Warrick, 2010). Complicating matters, both theoretical and experimental evidence suggest that robust CPGs with similar activity patterns can have widely variable underlying cell intrinsic and synaptic conductances (Prinz et al., 2004; Marder and Goaillard, 2006; Schulz et al., 2006; Schulz et al., 2007; Goaillard et al., 2009; Norris et al., 2011; Roffman et al., 2011). These individually variable circuits, nevertheless, must be reliable, and it remains an open question how such circuits respond and adapt to environmental challenges.

In the context of neuronal circuits, global perturbations involve changes to properties of the environment in which the neurons reside and thus may exert a wide influence over most circuit neurons. For instance, changes in temperature and pH will influence cellular function by altering how basic biochemical processes occur. Global perturbations also include changes to the ionic composition of extracellular fluid that then alter the electrochemical driving forces important for neuronal activity. In particular, elevated extracellular potassium concentration ($[K^+]$), is a physiologically relevant depolarizing stimulus associated with a wide array of conditions including thermal stress, epileptic seizures, kidney failure, traumatic brain injury, and stroke (Baylor and Nicholls, 1969; Katayama et al., 1990; Pérez-Pinzón et al., 1995; Jensen and Yaari, 1997; Rodgers et al., 2007; Krishnan and Kiernan, 2009; Morrison et al., 2011;

Arnold et al., 2014; Chauvette et al., 2016). Experimentally, increased extracellular [K^+] is often used to induce changes in neuronal activity. For instance, in rodent hippocampal cultures, increased [K^+] were used to depolarize neurons and activate calcium-dependent transcription pathways (Lin et al., 2008; Sharma et al., 2015). Increased [K^+] is often applied to pre-Bötzinger complex neurons in acute slice preparations to reestablish rhythmic firing lost in the absence of excitatory inputs (Ballerini et al., 1999; Panaitescu et al., 2009; Ruangkittisakul et al., 2011; Rybak et al., 2014). Although our understanding of the basic depolarizing effect of increased [K^+] on neuronal membrane potential is well defined (Somjen, 1979), the circuit level and long-term consequences of global changes in [K^+] are less well understood. Here, we characterized the effects of increased [K^+] on a well described motor circuit of the crab, *Cancer borealis*.

The crustacean stomatogastric nervous system (STNS) has been extensively studied and is a highly advantageous system for the study of fundamental mechanisms of circuit dynamics, pattern generation, and neuromodulation (Selverston, 1976; Selverston and Moulins, 1987; Marder and Bucher, 2007; Marder et al., 2014). The combination of intrinsic variability, well-established connectivity, and production of behaviorally relevant fictive activity, make the STNS an attractive model to study underlying network dynamics and robustness in response to a global perturbation (Selverston and Miller, 1980; Eisen and Marder, 1982; Miller and Selverston, 1982; Selverston et al., 1982). Previous studies have shown that the pyloric rhythm of the STNS is extraordinarily robust to changes in both temperature and pH (Tang et al., 2010; Tang et al., 2012; Soofi et al., 2014; Marder et al., 2015; Haddad and Marder, 2018; Haley et al., 2018; Kushinsky et al., 2019). Extracellular potassium concentrations

102 can act on all neurons in a circuit simultaneously and affect a multitude of cellular
103 processes, making it an attractive model with which to study the effects of a global
104 perturbation on neural circuits (Somjen, 2002; Misonou et al., 2004).

105 Here, we characterize the effects of elevated [K^+] on the pyloric rhythm and
106 quantify the time course of these effects. We describe both some expected and
107 unanticipated effects of the treatment.

Materials and Methods

Animals and dissections

Adult male Jonah Crabs, *Cancer borealis*, (N = 73) were obtained from Commercial Lobster (Boston, MA) between December 2016 and March 2019 and maintained in artificial seawater at 10-12˚C in a 12-hour light/dark cycle. On average, animals were acclimated at this temperature for one week before use. Prior to dissection, animals were placed on ice for at least 30 min. Dissections were performed as previously described (Gutierrez and Grashow, 2009). In short, the stomach was dissected from the animal and the intact stomatogastric nervous system (STNS) was removed from the stomach including the commissural ganglia, esophageal ganglion and stomatogastric ganglion (STG) with connecting motor nerves. The STNS was pinned in a Sylgard-coated (Dow Corning) dish and continuously superfused with 11˚C saline.

Solutions

Physiological *Cancer borealis* saline was composed of 440 mM NaCl, 11 mM KCl, 26 mM $MgCl_2$, 13 mM $CaCl_2$, 11 mM Trizma base, 5 mM maleic acid, pH 7.4-7.5 at 23˚C (approximately 7.7-7.8 pH at 11˚C). High - 1.5x, 2x, 2.5x, and 3x[K^+] - salines (16.5, 22, 27.5 and 33mM KCl respectively) were prepared by adding more KCl salt to the normal saline formula. Picrotoxin (PTX) used to block glutamatergic synapses was added to normal or 2.5x[K^+] saline at a 10^{-5}M concentration for isolated pacemaker experiments (Marder and Eisen, 1984).

Electrophysiology

Intracellular recordings from somata were performed in the desheathed STG with 10–30 MΩ sharp glass microelectrodes filled with internal solution (10 mM $MgCl_2$, 400 mM potassium gluconate, 10 mM HEPES buffer, 15 mM $NaSO_4$, 20 mM NaCl (Hooper et al.,

2015). Intracellular signals were amplified with an Axoclamp 900A amplifier (Molecular Devices, San Jose). Extracellular nerve recordings were made by building wells around nerves using a mixture of Vaseline and mineral oil and placing stainless-steel pin electrodes within the wells to monitor spiking activity. Extracellular nerve recordings were amplified using model 3500 extracellular amplifiers (A-M Systems). Data were acquired using a Digidata 1440 digitizer (Molecular Devices, San Jose) and pClamp data acquisition software (Molecular Devices, San Jose, version 10.5). For identification of Pyloric Dilator (PD) and Lateral Pyloric (LP) neurons, somatic intracellular recordings were matched to action potentials on the pyloric dilator nerve (*pdn*), lateral pyloric nerve (*lpn*) and/or the lateral ventricular nerve (*lvn*).

Elevated [K^+] saline application

Prior to all applications of elevated [K^+] saline, baseline activity was recorded for 30 minutes in physiological saline. Following the baseline recording, the entire preparation was superfused with elevated [K^+] saline in concentrations ranging from 1.5x to 3x [K^+] for 90 minutes. The preparation was then washed with physiological saline for 30 minutes. Recordings from PD neurons in the isolated pacemaker kernel were made by superfusing with 10^{-5}M Picrotoxin (PTX) saline until all inhibitory synaptic potentials in the PD neurons disappeared (for at least 20 minutes). These preparations were then exposed to 2.5x[K^+] PTX saline for 90 minutes, followed by a 30-minute wash in PTX saline.

Threshold and excitability measurements

To measure the action potential threshold and excitability of PD neurons, two-electrode current clamp was used to apply slow ramps of current from -4nA to +2nA over 60s. Resting membrane potential and input resistance were measured during both baseline

conditions and after the application of elevated [K^+] to ensure the integrity of the preparation (neurons with input resistances <4MΩ were discarded). Three ramps were performed during baseline at 10-minute intervals, and ramps were performed in 2.5x[K^+] at 5, 10, 20, 30, 40, 50, 60, 70, 80 and 90 minutes after the start of elevated [K^+] superfusion. After the preparation was returned to physiological saline, three ramps were performed again at 10-minute intervals. In recordings from the PD neurons with glutamatergic synapses blocked by PTX, baseline ramps were performed as described above, followed by three ramps in PTX saline. Preparations were then superfused with 2.5x[K^+] PTX saline and washed in PTX saline following the same ramp procedure as above.

Data acquisition and analysis

Recordings were acquired using Clampex software (pClamp Suite by Molecular Devices, San Jose, version 10.5) and were visualized and analyzed using custom MATLAB waveform analysis scripts. These scripts were used to detect and measure voltage response amplitudes and membrane potentials, plot raw recordings and processed data, generate spectrograms, and perform some statistical analyses.

Spectral analysis

Spectrograms were calculated using the Burg (1967) method for estimation of the power spectrum density in each time-window. The Burg method (1967) fits the autoregressive (AR) model of a specified order p in the time series by minimizing the sum of squares of the residuals. The fast-Fourier transform (FFT) spectrum is estimated using the previously calculated AR coefficients. This method is characterized by higher resolution in the frequency domain than traditional FFT spectral analysis, especially for a relative short time window (Buttkus, 2000). We used the following parameters for the spectral

estimation: data window of 3.2 s, 50% overlap to calculate spectrogram, number of estimated AR-coefficients p=window/4+1. Before the analysis, voltage traces were low pass filtered to 5 Hz using a six-order Butterworth filter and down-sampled. PD neuron burst frequency was calculated as the mean frequency at the peak spectral power in each sliding window.

Analysis of interspike interval distributions

Intracellular voltage traces were thresholded to obtain spike times. Distributions of inter-spike intervals (ISIs) were calculated within 2-minute bins. Hartigan's dip test of unimodality (Hartigan and Hartigan, 1985) was used to obtain the dip statistic for each of these distributions. This dip statistic was compared to Table 1 in Hartigan and Hartigan (1985) to find the probability of multi-modality. The test creates a unimodal distribution function that has the smallest value deviations from the experimental distribution function. The largest of these deviations is the dip statistic. The dip statistic shows the probability of the experimental distribution function being bimodal. Larger value dips indicate that the empirical data are more likely to have multiple modes (Hartigan and Hartigan, 1985).

Activity pattern plots

For all recordings, we determined the time of spikes over the course of the experiment. For the recovery time plots, silence was defined as no more than 2 spikes in a 30-second sliding window. Otherwise, all spike behaviors (even if irregular) were counted as active spiking.

To more broadly determine the activity pattern of each PD neuron across the experiment, we analyzed the distribution of inter-spike intervals (ISI) in 2-minute bins using Hartigan's dip statistic, as described above. If the dip statistic was 0.05 or higher

the neuron was considered to be bursting. If the dip statistic was lower than 0.05 the neuron was considered to be tonically firing. Neurons with some spikes, but not enough ISIs to calculate the dip, were classified as sparsely firing. Neurons with no ISIs in the observed window were classified as silent. We then plotted the activity pattern of the neuron in these four categories – bursting, tonic, sparse firing and silent – for each PD neuron across the entire experiment.

Identification of the spike threshold

The spike threshold was identified as the voltage point of the maximum curvature before the first spike. Specifically, we calculated the first derivative of the voltage (dV/dt) and defined the spike onset as the point when dV/dt crosses the threshold value of 10 mV/ms.

All electrophysiology analysis scripts are available at the Marder lab GitHub (https://github.com/marderlab).

Results

Network activity in the pyloric circuit

The entire stomatogastric nervous system (STNS) of the crab *Cancer borealis* was isolated intact from the stomach and pinned in a dish, allowing us to change the composition of the continuously flowing superfused saline (Fig.1A). The stomatogastric ganglion (STG) contains identified neurons that drive the pyloric rhythm that filters food through the animal's foregut. Figure 1B illustrates the stereotypical triphasic pyloric pattern which is comprised of the activity from lateral pyloric (LP), pyloric (PY) and pyloric dilator (PD). The rhythm is recorded extracellularly from motor axons contained in the lateral ventricular nerve (*lvn*) and other nerves. Figure 1C illustrates the connectivity diagram of the pyloric network. The anterior burster (AB) neuron, the intrinsic oscillator that drives the circuit, is strongly electrically coupled to two PD neurons, which burst synchronously with the AB neuron. Together the AB and two PD neurons form the pacemaker kernel of the network, and their coordinated burst of spikes initiates each triphasic cycle (Maynard, 1972). Synaptic connections between neurons in the STG are all inhibitory and are both graded and spike mediated (Graubard et al., 1980; Manor et al., 1997). Rhythmic inhibition from the pacemaker drives bursting activity resulting from post-inhibitory rebound in the LP neuron and PY neurons which reciprocally inhibit each other (Hartline and Gassie, 1979; Selverston and Miller, 1980). As a result, LP bursting and PY bursting compose the second and third phases of the pyloric rhythm respectively.

The pyloric rhythm is disrupted by high extracellular potassium

To test the response of the pyloric rhythm to changes in extracellular [K^+], we switched from superfusion of normal physiological saline to superfusion of saline with elevated [K^+] over the STNS while continuously recording the activity of pyloric neurons extracellularly from the *lvn*. We tested concentrations of [K^+] that were 1.5, 2, 2.5 and 3-times physiological concentrations to study the dose-dependent responses of pyloric neurons to changes in extracellular [K^+]. When extracellular [K^+] was changed slightly, to 1.5x the physiological concentration (Fig. 1*D*, N = 4), the pyloric rhythm remained triphasic and was negligibly affected. When exposed to 2x [K^+] (Fig. 1*E,* N = 20), the response of pyloric neurons was more variable; in some cases (N = 9/20) there was a short disruption of the triphasic pyloric rhythm, which was followed by the recovery of spiking activity.

Higher concentrations of extracellular [K^+] produced more pronounced effects on pyloric activity. Superfusion of 2.5x [K^+] (Fig. 1*F,* N = 12 extracellular recordings) reliably and profoundly altered the pyloric rhythm. During the application of 2.5x[K^+] saline, all preparations exhibited a surprising disruption of action potentials from pyloric neurons, followed by recovery of spiking activity during continued exposure to 2.5x[K^+] saline. Similarly, application of 3x[K^+] saline to the STNS resulted in consistent cessation of the pyloric rhythm (Fig. 1*G,* N = 5). However, at 3x[K^+], very few of the preparations recovered consistent activity. Based on these responses, we settled on a concentration of 2.5 times the control saline K^+ concentration (2.5x[K^+]) for further study, which reliably disrupted the pyloric rhythm and was accompanied by a consistent recovery of spiking or bursting activity during the continued application of 2.5x[K^+].

The pattern of loss and recovery of pyloric activity in 2.5x[K^+] saline was consistent across all experiments; however, the precise nature of each neuron's response

cannot be determined from extracellular data alone. Therefore, to obtain more detailed information on the effects of increased [K^+], we recorded intracellularly from pyloric neurons while superfusing 2.5x[K^+] saline over the STNS.

Pyloric neurons PD and LP depolarize and temporarily lose spiking activity in high extracellular potassium

With intracellular recordings, we saw a marked loss of spiking activity (crash) of pyloric neurons in response to the application of 2.5x[K^+] saline that was consistent with the previously described extracellular recordings. In the representative example shown in Figure 2, the PD and LP neurons burst robustly in normal physiological saline (Fig. 2*Ai*). Within a few minutes of the start of 2.5x[K^+] saline application, the minimum membrane potential of the PD and LP neurons depolarized by 15 and 22mV respectively (Fig. 2*Aii*), which was coincident with a reduction in firing frequency. The activity of both the LP and PD neurons became more burst-like over the course of the 90-minute application of 2.5x[K^+] saline (Fig. 2*Aiii-iv*) and recovered to normal baseline behavior when returned to physiological saline (Fig. 2*Av*). The pattern of depolarization and recovery of spiking can be more clearly depicted by plotting time-condensed voltage traces for the PD neuron (the response of the LP neuron closely resembles that of the PD neuron) for the entire 150 minute experiment. In this trace, the membrane potential depolarizes in 2.5x[K^+] saline followed by a loss of spiking activity (Fig. 2*B*). To visualize spiking behavior over the course of the experiment, we plotted the instantaneous interspike intervals (ISI) of the PD neuron for the whole experiment on a log scale ($\log_{10}$(ISIs), Fig. 2*C*). All healthy PD neurons in physiological saline have regular bursting activity that yields a bimodal distribution of ISIs, reflecting the relatively longer

ISI period between bursts and the shorter ISIs of spikes within a burst. Although the initial depolarization in 2.5x[K^+] saline caused a very brief increase in burst and spike frequency, the increase was immediately followed by a loss of all spiking activity (Fig. 2*C*). Over the course of the 2.5x[K^+] saline application, both the PD and LP neuron recovered rhythmic bursts of action potentials, which is clear from the re-emergence of two ISI bands (Fig. *2C)*. Bursting activity is suggestive of the re-appearance of slow membrane potential oscillations. These slow oscillations are best visualized by spectrograms of the neuron's membrane potential; recovery of bursting activity in elevated [K^+] saline can be seen by the re-appearance of a strong frequency band in the voltage spectrogram (Fig. *2D*). We then calculated the most hyperpolarized point of the membrane potential in each burst averaged over five-minute bins for all PD neurons to determine the overall depolarizing effect of 2.5x[K^+] saline. Individual PD neurons depolarized upon application of 2.5x[K^+] saline and remained depolarized throughout the application with no repolarization of the membrane potential (Fig. 2*E*). Over all preparations, PD neurons depolarized upon application of 2.5x[K^+] saline (Fig. 2*F,* repeated measures ANOVA, Tukey post-hoc $p<0.05$, average depolarization after 10 minutes 14.5 ± 3.3mV) After the initial change in the first 10 minutes in 2.5x[K^+], the minimum membrane potentials did not change for the remainder of the elevated [K^+] application ($p > 0.05$). The minimum membrane potential returned to baseline levels when the preparations were returned to physiological saline (n.s., $p > 0.05$). The behavior of LP neurons in 2.5x[K^+] was very similar to that of PD neurons; LP neurons depolarized by 16.5 ± 2.9mV after 10 minutes in 2.5x[K^+] ($n = 5$) and remained depolarized for the duration of the elevated [K^+] application.

Variability in the response of PD neurons to 2.5x[K^+] saline

Although pyloric activity and circuit connectivity is highly conserved across animals, responses of individual PD neurons to 2.5x[K^+] saline varied substantially across preparations. Superfusion of 2.5x[K^+] saline led to a period of silence in 9 of the 13 PD neurons, with striking variability in the duration of silence and extent of recovery across animals. Figure 3 shows the responses of four PD neurons from four different animals to a 90-minute application of 2.5x[K^+] saline. Across all preparations (n = 13), the time of silence elicited by 2.5x[K^+] saline application varied from 1 to 62 minutes (time of silence was 10.9 ± 5.8 minutes SD). We characterized the recovery of PD neuron activity by comparing the ISI distributions over time. In some cases, the PD neurons exhibited only tonic firing activity in 2.5x[K^+] saline which is reflected by the presence of a single ISI band (Fig. 3*A, B*). In other cases, PD neurons regained burst-like activity, which was reflected in the re-emergence of two ISI bands in 2.5x[K^+] saline (Fig. 3*C, D*).

In all PD neuron recordings, the variable period of silence upon application of 2.5x[K^+] saline was followed by the recovery of spiking activity. For all PD neurons, we calculated the "time to recovery," defined as the length of time between the silencing of the neuron and when the neuron recovered at least two action potentials in a 30-second sliding window during the application of 2.5x[K^+] saline. We were interested in determining whether aspects of baseline activity of each PD neuron influenced the neuron's time to recovery. Therefore, for each PD neuron, we calculated the mean minimum membrane potential during baseline recordings (Fig. 3*E*), the change in membrane potential upon application of 2.5x[K^+] saline (Fig. 3*F*) and the baseline bursting frequency (Fig. 3*G*) and compared these values to the time to recovery for each

corresponding neuron. We found no correlation between any of these values and the time elapsed until recovery of spiking activity (R^2=0.203, R^2=0.104, R^2=0.012 respectively).

PD neurons in the isolated pacemaker kernel continue spiking in 2.5x[K^+] saline

From the previous experiments, it was unclear to what extent the crash and recovery of activity in 2.5x[K^+] saline was due to presynaptic inputs to PD neurons. Because the PD and AB neurons receive only glutamatergic input from other pyloric network neurons, the pacemaker kernel can be studied in isolation from the pyloric network neurons by superfusing saline with 10^{-5}M picrotoxin (PTX), which blocks ionotropic glutamatergic synapses in the STG (Fig. 4*A*) (Bidaut, 1980).

The response of PD neurons in the presence of PTX (PTX(+)) to 2.5x[K^+] saline was markedly different from the behavior of PD neurons in control conditions (in the absence of PTX) (PTX(-)). Figure 4 illustrates a representative example of the responses of PD neurons to 2.5x[K^+] PTX saline; the preparation initially switched from rhythmic bursting to tonic spiking activity in 2.5x[K^+] PTX saline (Fig. 4*Biii*), followed by recovery of bursting activity that became more pronounced with time (Fig. 4*B iv – vi*). There was no interruption of (firing) activity upon the superfusion of 2.5x[K^+] PTX saline (Fig. 4C) in PD neurons as compared to 25.x[K^+] alone. The recovery of bursting in 2.5x[K^+] PTX saline can also be seen in the emergence of two distinct ISI bands (Fig. 4*D*) and the emergence of a robust frequency band in the spectrogram of the PD intracellular voltage trace (Fig. 4*E*).

We further quantified the response of PD neurons to 2.5x[K^+] PTX saline by calculating the mean minimum membrane potential in five-minute bins for each neuron across the experiment (n = 8, Fig. 4*F*). Similar to PD neurons in the intact circuitry, all PTX(+) PD neurons depolarized in 2.5x[K^+] saline (Fig. *4G,* repeated measures ANOVA, Tukey post-hoc $p < 0.05$, average depolarization after 10 minutes 12.6 ± 3.0mV). The minimum membrane potential of PD neurons in PTX then remained stable during the application of 2.5x[K^+] and returned to baseline levels when returned to physiological extracellular [K^+] (Fig. *4G,* $p > 0.05$). Importantly, the fact that PTX(+) PD neurons maintain tonic firing upon the application of 2.5x[K+] saline despite marked depolarization indicates that the crash observed in PTX(-) PD neurons is unlikely to be due to depolarization block.

Synaptic inputs alter response of PD neurons to 2.5x[K^+] saline

The initial responses of PD neurons to 2.5x[K^+] saline application differed in the presence or absence of PTX. This difference indicates the existence of a circuit-driven response to elevated [K^+]. To quantify this effect, we used values from the Hartigan's dip test on 2-minute bins of log(ISI) to determine the time that each PD neuron was either bursting, tonically firing, or silent throughout the experiment and plotted the activity of each PD neuron over time (see methods).

In the intact circuit, the majority (N = 9 of 13) of PD neurons exhibited a period of silence following the application of 2.5x[K^+] saline, then recovered spiking activity over a variable amount of time (Fig. 5*A*). In 2.5x[K^+] PTX saline, PD neurons either remained active or only briefly went silent, then demonstrated robust recovery of spiking or bursting activity (Fig. 5*B*). The average time of PD silence in 2.5x[K^+] saline

was significantly different with the addition of PTX (Fig. 5*C*, Wilcoxon rank-sum test p = 0.013), as was the average time of PD sparse firing between PTX(+) and PTX(-) PD neurons (Fig. 5*D*, Wilcoxon rank-sum test p = 0.034). In both the time of silence and sparse firing comparisons, the difference between PTX(+) and PTX(-) PD neurons was still significant when the largest point in the PTX(-) group was removed. Neither the average time of tonic firing (Fig. 5*E*, n.s., p = 0.77), nor the average time of burst firing significantly were significantly different in the presence or absence of PTX (Fig. 5*F*, n.s., p = 0.51).

Excitability of PD neurons changes rapidly during exposure to 2.5x[K^+] saline

We wished to see whether periods of silence in high K^+ were due to depolarization block. Therefore, we applied 60 second steady ramps of current from -4nA to +2nA to PD neurons at several time points during the period of silence elicited by application of 2.5x[K^+] saline. In silent PD neurons, action potentials could always be induced by injecting positive current, indicating that this period of silence is not due to depolarization block (Fig. 6A, ramps at 5-minutes and 10-minutes).

To determine the excitability of PD neurons during application of 2.5x[K^+], we repeated the slow current ramps from -4nA to +2nA at 5, 10, 20, 30, 40, 50, 60, 70, 80, and 90 minutes after the beginning of the 2.5x[K^+] saline application in the presence or absence of PTX. In the representative example shown, there was a clear change in the number and frequency of spikes elicited in the PD neuron by the current ramp as a function of time in 2.5x[K^+] saline (Fig. 6*A*). In addition, as time in 2.5x[K^+] increased,

406 more spikes were elicited at the same membrane potentials during the current ramp
407 (Fig. 6*B*).

408 For each individual PTX(-) preparation (N = 5), spike threshold became more
409 hyperpolarized in the PD neuron as a function of time in 2.5x[K^+] saline (Fig. 6*C*). In
410 contrast, when the same current ramps were applied to PTX(+) PD neurons (N = 6),
411 there was no clear trend in spike threshold as a function of time in 2.5x[K^+] saline (Fig.
412 6*D*). Across all PD neurons, we calculated the percent change in spike threshold from
413 baseline for each current ramp. There was a significant drop in spike threshold over
414 time for PD neurons in 2.5x[K^+] saline between the 5-minute the 60 through 90-minute
415 time points and also between the 10-minute and the 60 through 90-minute time points
416 (Fig. *6F* blue, one-way repeated measures ANOVA, Tukey Post-Hoc test, all $p < 0.05$).
417 For most of these neurons the biggest changes in firing rates and spike threshold
418 occurred during the first 10 minutes of 2.5x[K^+] saline application, which is similar to
419 the time in which most PD neurons recover spiking activity in elevated [K^+]. Across all
420 PTX(+) PD neurons there was no significant percent change in spike threshold over
421 time in 2.5x[K^+] (Fig. *6G* red, one-way repeated measures ANOVA, Tukey Post-Hoc test,
422 n.s., all $p > 0.05$).

423 To visualize overall changes in PD neuron excitability, we then calculated average
424 F-I curves for all neurons at the beginning (5-minute ramp) and end (90-minute ramp)
425 of the 2.5x[K^+] saline application. Control PD neurons become more excitable as time in
426 2.5x[K^+] increases; there is a shift in the average F-I curve between the 5- and 90-
427 minute time points (Fig. 6*F* solid lines, two-way repeated measures ANOVA, $p = 0.009$).
428 In addition, at the 5-minute time point in 2.5x[K^+], PTX(+) PD neurons are more
429 excitable than PTX(-) PD neurons (Fig 6*F* purple lines, two-way repeated measures

ANOVA, p = 0.036). This initial difference in excitability is consistent with the fact that PTX(+) neurons remain active upon application of 2.5x[K^+], while PTX(-) PD neurons typically lose spiking activity. The excitability of PTX(+) PD neurons does not change over time in 2.5x[K^+]; there was no significant difference between the 5- and 90-minute PTX(+) PD neuron F-I curves (Fig 6*F* dashed lines, two-way repeated measures ANOVA, p = 0.097). In addition, by the end of the 2.5x[K^+] application (90-minutes), there was no significant difference between the F-I curves of PTX(+) and PTX(-) PD neurons (Fig 6*F* red lines, two-way repeated measures ANOVA, p = 0.375).

Discussion

Surprising inhibitory effect of a depolarizing stimulus

In the STG, the pyloric rhythm is robust to multiple perturbations including changes in temperature, pH and neuromodulatory state (Tang et al., 2010; Tang et al., 2012; Temporal et al., 2014; Hamood et al., 2015; Haddad and Marder, 2018; Haley et al., 2018). Here, we tested whether pyloric neurons are similarly robust to global depolarization through changes to extracellular [K^+]. It is generally assumed that positive current input or depolarization of a neuron's membrane potential will lead to an increase in neuronal activity, and that extreme depolarizations can lead to loss of activity through depolarization block. Instead, we found a type of transient neuronal silence in response to elevated [K^+] that is not due to a depolarization block.

In the pyloric circuit, all local synaptic connections are inhibitory (Eisen and Marder, 1982; Miller and Selverston, 1982). Synaptic transmission in the STG is both graded and spike-mediated, meaning that action potentials are not required for inhibitory synapses to function (Graubard et al., 1980; Manor et al., 1997; Nadim et al., 1997). Therefore, the observed decrease in both bursting and spiking activity in elevated extracellular [K^+] may be caused by global depolarization leading to an increase in graded inhibition that suppresses spiking and bursting activity. In support of this theory, elevated [K^+] does not have the same inhibitory effect on PD neurons with glutamatergic synapses blocked compared to PD neurons with intact synaptic connections. Similarly, in the proprioceptive neurons of the blue crab and the muscle receptor organ of the crayfish, it was recently reported that increased [K^+] also has an inhibitory effect at concentrations not thought to cause a depolarization block (Malloy et al., 2017).

462

463 **Adaptation to global perturbation**

464 The PD/AB pacemaker unit of the pyloric circuit exhibited rapid adaptation to
465 the disruptive stimulus of increased extracellular [K^+]. Although the triphasic pyloric
466 rhythm was not fully restored in 2.5x[K^+] saline, PD neurons exhibited rapid changes in
467 excitability over several minutes, which corresponded to the recovery of spiking and, in
468 many cases, bursting activity.

469 Classical homeostatic plasticity takes place over hours to days and requires
470 changes in intracellular calcium concentrations which then subsequently drive changes
471 in gene expression, leading to cell-intrinsic changes in excitability (Desai et al., 1999;
472 Cudmore and Turrigiano, 2004; Turrigiano, 2012). There is evidence that this
473 mechanism can be induced by changes in extracellular [K^+]. Rat myenteric neurons
474 cultured in elevated [K^+] serum for several days exhibit long-lasting changes in Ca^{2+}
475 channel function (Franklin, 1992). Similarly, culturing rat hippocampal pyramidal cells
476 in high [K^+] medium for several days leads to activation of calcium-dependent changes
477 in input resistance and the resting membrane potential that regulates the intrinsic
478 excitability of the neurons (O'Leary et al., 2010). Changes in K^+ channel densities are
479 also associated with homeostatic regulation of neuronal activity. Depolarization of
480 crustacean motor neurons with current pulses for several hours alters K^+ channel
481 densities in a cell-specific manner through a calcium-dependent mechanism (Golowasch
482 et al., 1999). In addition, cerebellar granule cells in which inhibitory GABA receptors are
483 blocked for several days maintain their response to excitatory input by strengthening
484 voltage-independent K^+ conductances (Brickley et al., 2001). Adaptation to global
485 perturbation over several hours to days is well described by models via calcium signals

that influence expression levels of ion channels (O'Leary et al., 2014; O'Leary, 2018). Pyloric neurons in the STG also exhibit these long-term adaptations; preparations in which neuromodulatory inputs are removed initially lose rhythmicity and gradually recover over the course of several days (Thoby-Brisson and Simmers, 1998, 2002; Luther et al., 2003; Gray and Golowasch, 2016; Gray et al., 2017).

Intriguingly, many cases of rapid adaptation in neuronal circuits are related to changes in signaling between neurons. At the *Drosophila* neuromuscular junction, blocking glutamatergic signaling results in long-lasting changes in synaptic strength within minutes (Frank et al., 2006; Müller and Davis, 2012; Müller et al., 2012). In the crustacean cardiac ganglion, blocking delayed rectifier K^+ currents led to adaptation of the circuit and an increase in electrical coupling strength within one hour (Lane et al., 2016). Although these rapid changes in synaptic strength are often associated with Hebbian plasticity and learning, rapid alterations in synapses can also lead to a homeostatic-like maintenance of circuit activity.

The rapid adaptation of PD neurons in elevated extracellular [K^+] is most likely due to a combination of cell-intrinsic conductance changes and synaptic modulation. In crustacean motor neurons, cell-intrinsic changes in current densities have been shown to be modulated by second-messenger kinase pathways activated by global depolarization (Ransdell et al., 2012). Rapid changes in circuit state could also be influenced by neuromodulation, as these experiments were conducted with the entire STNS, including connections to the upstream modulatory ganglia which were also exposed to the elevated [K^+]. In the STNS, the upstream commissural ganglia and the esophageal ganglion release a wide range of neuromodulators onto the STG that affect excitability of cells and the pyloric rhythm (Marder and Bucher, 2007; Marder, 2012). In

510 particular, proctolin released by the MPN and MCN1 neurons endogenously drives the
511 pyloric pacemaker neuron AB (Hooper and Marder, 1987; Nusbaum and Marder, 1989;
512 Wood et al., 2000; Stein et al., 2007). Dopamine is also released by modulatory neurons
513 in the STNS, and exogenous application of dopamine can cause rapid changes in
514 electrical coupling strength and has been shown to rapidly regulate potassium currents
515 in both mammalian and invertebrate neurons (Tornqvist et al., 1988; Harris-Warrick et
516 al., 1998; Gruhn et al., 2005; Rodgers et al., 2013).
517
518 **Variable responses to similar perturbations**
519 The effects of perturbations are often represented by averaging the experimental
520 results from a number of individuals, but there are several reasons why this approach is
521 not always appropriate. Circuits with apparently identical outputs under control
522 conditions can present distinctly different responses to perturbation due to underlying
523 differences in network parameters (Tang et al., 2012; Hamood and Marder, 2014;
524 Haddad and Marder, 2018; Haley et al., 2018; Alonso and Marder, 2019). Indeed, in this
525 study we observed a wide range of responses in identified PD neurons to the same
526 experimental conditions, 2.5x[K^+], which may uncover individual differences that are
527 not evident during control conditions. Within the STG, conductance densities and
528 strengths of synaptic connections can vary up to five-fold in magnitude between
529 individuals (Schulz et al., 2006; Schulz et al., 2007; Goaillard et al., 2009; Shruti et al.,
530 2014; Temporal et al., 2014). Variability in neuronal conductances underlying similar
531 activity patterns has also been demonstrated across phyla (Swensen and Bean, 2005;
532 Nelson and Turrigiano, 2008; Tran et al., 2019). In addition, computational modeling of
533 the pyloric network revealed that multiple combinations of independent circuit

parameters can give rise to functionally identical activity patterns (Goldman et al., 2001; Prinz et al., 2004; Taylor et al., 2009; Marder et al., 2015). The application of elevated [K^+] saline to identified STG neurons provides additional evidence that differences in individual conductance parameters influence circuit responses to global perturbation (Alonso and Marder, 2019).

Implications for disease states

Hyperkalemia is well documented in many nervous system disorders; however, it remains unclear how the changes in [K^+] acutely affect neuronal activity. Chronic Kidney Disease (CKD) leads to increases in serum [K^+] up to three times normal levels, directly affecting neuronal excitability, and changes in neuronal properties (Krishnan and Kiernan, 2009; Arnold et al., 2014). Similarly, increased activity of a group of neurons can increase the extracellular [K^+] in the surrounding tissue (Baylor and Nicholls, 1969; Kříž et al., 1974) and epileptic seizures and brain trauma can lead to increases in [K^+] in surrounding brain regions (Moody et al., 1974; Katayama et al., 1990; Silver and Erecinska, 1994; Fröhlich et al., 2008). These transient changes in extracellular [K^+] have been tied to long lasting changes in the organization and phosphorylation pattern of K^+ channels (Misonou et al., 2004), which could lead to long-lasting changes in circuit function (Somjen, 2001, 2002; Rodgers et al., 2007).

In this study, pyloric neurons respond to elevated [K^+] with a rapid adaptation of excitability; another example of how the such adaptations occur. The fast adaptation of pyloric neurons to global changes in [K^+] also suggests that rapid swings in [K^+] may be more damaging to neurons than gradual shifts or sustained changes in concentration.

Reassessing global perturbation

The results of this study highlight the unexpected complexity of seemingly simple perturbations. In this classical manipulation of increased extracellular [K^+] we observed a paradoxical decrease in the activity of PD neurons upon bath application of high [K^+], followed by a recovery of activity in a short period time. Despite knowing the network connectivity, circuit properties and behavior of identified neurons within the STG, we were still unable to predict or fully explain the effects of increased [K^+] on circuit performance. The complex interaction between circuit level effects and cell intrinsic responses to simple changes in ion concentrations underscores the importance of recording and reporting neuronal activity during such manipulations in any experiment.

References

Alonso LM, Marder E (2019) Visualization of currents in neural models with similar behavior and different conductance densities. eLife 8:e42722.

Arnold R, Pussell BA, Howells J, Grinius V, Kiernan MC, Lin CSY, Krishnan AV (2014) Evidence for a causal relationship between hyperkalaemia and axonal dysfunction in end-stage kidney disease. Clin Neurophysiol 125:179-185.

Ballerini L, Galante M, Grandolfo M, Nistri A (1999) Generation of rhythmic patterns of activity by ventral interneurones in rat organotypic spinal slice culture. J Physiol 517:459-475.

Baylor DA, Nicholls JG (1969) Changes in extracellular potassium concentration produced by neuronal activity in the central nervous system of the leech. J Physiol 203:555-569.

Bidaut M (1980) Pharmacological dissection of pyloric network of the lobster stomatogastric ganglion using picrotoxin. J Neurophysiol 44:1089-1101.

Brickley SG, Revilla V, Cull-Candy SG, Wisden W, Farrant M (2001) Adaptive regulation of neuronal excitability by a voltage- independent potassium conductance. Nature 409:88-92.

Burg JP (1967) Maximum entropy spectral analysis. In: Proc. 37th Meeting Society of Exploration Geophysicist. Oklahoma City, OK.

Buttkus B (2000) Spectral Analysis and Filter Theory. Berlin: Springer.

Chauvette S, Soltani S, Seigneur J, Timofeev I (2016) *In vivo* models of cortical acquired epilepsy. Neurosci Methods 260:185-201.

Cudmore RH, Turrigiano GG (2004) Long-term potentiation of intrinsic excitability in LV visual cortical neurons. J Neurophysiol 92:341-348.

590 Desai NS, Rutherford LC, Turrigiano GG (1999) Plasticity in the intrinsic excitability of cortical
591 pyramidal neurons. Nat Neurosci 2:515.
592 Eisen JS, Marder E (1982) Mechanisms underlying pattern generation in lobster stomatogastric
593 ganglion as determined by selective inactivation of identified neurons. III. Synaptic
594 connections of electrically coupled pyloric neurons. J Neurophysiol 48:1392-1415.
595 Frank CA, Kennedy MJ, Goold CP, Marek KW, Davis GW (2006) Mechanisms underlying the
596 rapid induction and sustained expression of synaptic homeostasis. Neuron 52:663-677.
597 Franklin JL (1992) Long-term Regulation of Neuronal Calcium Currents by Prolonged Changes of
598 Membrane Potential. J Neurosci 12:1726-1735.
599 Fröhlich F, Bazhenov M, Iragui-Madoz V, Sejnowski TJ (2008) Potassium dynamics in the
600 epileptic cortex: new insights on an old topic. The Neuroscientist 14:422-433.
601 Goaillard J-M, Taylor AL, Schulz DJ, Marder E (2009) Functional consequences of animal-to-
602 animal variation in circuit parameters. Nat Neurosci 12:1424-1430.
603 Goldman MS, Golowasch J, Marder E, Abbott L (2001) Global structure, robustness, and
604 modulation of neuronal models. J Neurosci 21:5229-5238.
605 Golowasch J, Abbott LF, Marder E (1999) Activity-dependent regulation of potassium currents
606 in an identified neuron of the stomatogastric ganglion of the crab *Cancer borealis*. J
607 Neurosci 19:RC33-RC33.
608 Graubard K, Raper JA, Hartline DK (1980) Graded synaptic transmission between spiking
609 neurons. Proc Natl Acad Sci USA 77:3733-3735.
610 Gray M, Golowasch J (2016) Voltage dependence of a neuromodulator-activated ionic current.
611 eneuro 3.

612 Gray M, Daudelin DH, Golowasch J (2017) Activation mechanism of a neuromodulator-gated
613 pacemaker ionic current. J Neurophysiol 118:595-609.
614 Gruhn M, Guckenheimer J, Land B, Harris-Warrick RM (2005) Dopamine modulation of two
615 delayed rectifier potassium currents in a small neural network. J Neurophysiol 94:2888-
616 2900.
617 Gutierrez GJ, Grashow RG (2009) *Cancer borealis* stomatogastric nervous system dissection.
618 JoVE (J Vis Exp):e1207.
619 Haddad SA, Marder E (2018) Circuit robustness to temperature perturbation is altered by
620 neuromodulators. Neuron 100:609-623. e603.
621 Haley JA, Hampton D, Marder E (2018) Two central pattern generators from the crab, *Cancer*
622 *borealis*, respond robustly and differentially to extreme extracellular pH. eLife 7:e41877.
623 Hamood AW, Marder E (2014) Animal-to-Animal Variability in Neuromodulation and Circuit
624 Function. Cold Spring Harbor Symp Quant Biol 79:21-28.
625 Hamood AW, Haddad SA, Otopalik AG, Rosenbaum P, Marder E (2015) Quantitative
626 reevaluation of the effects of short- and long-term removal of descending modulatory
627 inputs on the pyloric rhythm of the crab, *Cancer borealis*. eNeuro 2:0058-0014.
628 Harris-Warrick RM (2010) General principles of rhythmogenesis in central pattern generator
629 networks. Prog Brain Research 187:213-222.
630 Harris-Warrick RM, Johnson BR, Peck JH, Kloppenburg P, Ayali A, Skarbinski J (1998) Distributed
631 Effects of Dopamine Modulation in the Crustacean Pyloric Network a. Annals of the New
632 York Academy of Sciences 860:155-167.
633 Hartigan JA, Hartigan PM (1985) The dip test of unimodality. Ann Stat 13:70-84.

634 Hartline DK, Gassie DV, Jr. (1979) Pattern generation in the lobster (*Panulirus*) stomatogastric
635 ganglion. I. Pyloric neuron kinetics and synaptic interactions. Biol Cybern 33:209-222.
636 Hooper SL, Marder E (1987) Modulation of the lobster pyloric rhythm by the peptide proctolin. J
637 Neurosci 7:2097-2112.
638 Hooper SL, Thuma JB, Guschlbauer C, Schmidt J, Büschges A (2015) Cell dialysis by sharp
639 electrodes can cause nonphysiological changes in neuron properties. J Neurophysiol
640 114:1255-1271.
641 Jensen MS, Yaari Y (1997) Role of intrinsic burst firing, potassium accumulation, and electrical
642 coupling in the elevated potassium model of hippocampal epilepsy. J Neurophysiol
643 77:1224-1233.
644 Katayama Y, Becker DP, Tamura T, Hovda DA (1990) Massive increases in extracellular
645 potassium and the indiscriminate release of glutamate following concussive brain injury.
646 J Neurosurgery 73:889-900.
647 Krishnan AV, Kiernan MC (2009) Neurological complications of chronic kidney disease. Nat Rev
648 Neurol 5:542-551.
649 Kříž N, Syková E, Ujec E, Vyklický L (1974) Changes of of extracellular potassium concentration
650 induced by neuronal activity in the spinal cord of the cat. J Physiol 238:1-15.
651 Kushinsky D, Morozova E, Marder E (2019) *In vivo* effects of temperature on the heart and
652 pyloric rhythms in the Crab, *Cancer borealis*. J Exp Biol 222:jeb199190.
653 Lane BJ, Samarth P, Ransdell JL, Nair SS, Schulz DJ (2016) Synergistic plasticity of intrinsic
654 conductance and electrical coupling restores synchrony in an intact motor network.
655 eLife 5:e16879.

Lin Y, Bloodgood BL, Hauser JL, Lapan AD, Koon AC, Kim T-K, Hu LS, Malik AN, Greenberg ME (2008) Activity-dependent regulation of inhibitory synapse development by Npas4. Nature 455:1198-1204.

Luther JA, Robie AA, Yarotsky J, Reina C, Marder E, Golowasch J (2003) Episodic bouts of activity accompany recovery of rhythmic output by a neuromodulator-and activity-deprived adult neural network. J Neurophysiol 90:2720-2730.

Malloy C, Dayaram V, Martha S, Alvarez B, Chukwudolue I, Dabbain N, Mahmood DD, Goleva S, Hickey T, Ho A (2017) The effects of potassium and muscle homogenate on proprioceptive responses in crayfish and crab. J Exp Zool 327:366-379.

Manor Y, Nadim F, Abbott L, Marder E (1997) Temporal dynamics of graded synaptic transmission in the lobster stomatogastric ganglion. J Neurosci 17:5610-5621.

Marder E (2012) Neuromodulation of neuronal circuits: back to the future. Neuron 76:1-11.

Marder E, Eisen JS (1984) Transmitter identification of pyloric neurons: electrically coupled neurons use different transmitters. J Neurophysiol 51:1345-1361.

Marder E, Calabrese RL (1996) Principles of rhythmic motor pattern generation. Physiol Rev 76:687-717.

Marder E, Bucher D (2001) Central pattern generators and the control of rhythmic movements. Curr Biol 11:R986-R996.

Marder E, Goaillard JM (2006) Variability, compensation and homeostasis in neuron and network function. Nat Rev Neurosci 7:563-574.

Marder E, Bucher D (2007) Understanding circuit dynamics using the stomatogastric nervous system of lobsters and crabs. Annu Rev Physiol 69:291-316.

678 Marder E, Goeritz ML, Otopalik AG (2015) Robust circuit rhythms in small circuits arise from
679 variable circuit components and mechanisms. Curr Opin Neurobiol 31:156-163.
680 Marder E, Goeritz ML, Gutierrez GJ, Hamood A, Brookings T, Caplan J, Haddad S, Kispersky T,
681 Shruti S (2014) The Crustacean Stomatogastric Nervous System. Nervous Systems and
682 Control of Behavior 3:337-361.
683 Maynard DM (1972) Simpler networks. Annals of the New York Academy of Sciences 193:59-72.
684 Miller JP, Selverston AI (1982) Mechanisms underlying pattern generation in lobster
685 stomatogastric ganglion as determined by selective inactivation of identified neurons.
686 IV. Network properties of pyloric system. J Neurophysiol 48:1416-1432.
687 Misonou H, Mohapatra DP, Park EW, Leung V, Zhen D, Misonou K, Anderson AE, Trimmer JS
688 (2004) Regulation of ion channel localization and phosphorylation by neuronal activity.
689 Nat Neurosci 7:711-718.
690 Moody WJ, Jr. , Futamachi KJ, Prince DA (1974) Extracellular potassium activity during
691 epileptogenesis. Exp Neurol 42:248-263.
692 Morrison B, III, Elkin BS, Dollé J-P, Yarmush ML (2011) In vitro models of traumatic brain injury.
693 Ann Rev Biomedical Engineering 13:91-126.
694 Müller M, Davis GW (2012) Transsynaptic control of presynaptic Ca2+ influx achieves
695 homeostatic potentiation of neurotransmitter release. Curr Biol 22:1102-1108.
696 Müller M, Liu KSY, Sigrist SJ, Davis GW (2012) RIM controls homeostatic plasticity through
697 modulation of the readily-releasable vesicle pool. J Neurosci 32:16574-16585.

698 Nadim F, Manor Y, Abbott L, Marder E (1997) Strength and timing of graded synaptic
699 transmission depend on frequency and shape of the presynaptic waveform. In:
700 Computational Neuroscience, pp 19-22: Springer.
701 Nelson SB, Turrigiano GG (2008) Strength through diversity. Neuron 60:477-482.
702 Norris BJ, Wenning A, Wright TM, Calabrese RL (2011) Constancy and variability in the output of
703 a central pattern generator. J Neurosci 31:4663-4674.
704 Nusbaum MP, Marder E (1989) A modulatory proctolin-containing neuron (MPN). I.
705 Identification and characterization. J Neurosci 9:1591-1599.
706 O'Leary T, Williams AH, Franci A, Marder E (2014) Cell types, network homeostasis, and
707 pathological compensation from a biologically plausible ion channel expression model.
708 Neuron 82:809-821.
709 O'Leary T (2018) Homeostasis, failure of homeostasis and degenerate ion channel regulation.
710 Curr Opin Physiol 2:129-138.
711 O'Leary T, van Rossum MCW, Wyllie DJA (2010) Homeostasis of intrinsic excitability in
712 hippocampal neurones: dynamics and mechanism of the response to chronic
713 depolarization: Homeostatic regulation of intrinsic excitability. J Physiol 588:157-170.
714 Panaitescu B, Ruangkittisakul A, Ballanyi K (2009) Silencing by raised extracellular Ca^{2+} of pre-
715 Bötzinger complex neurons in newborn rat brainstem slices without change of
716 membrane potential or input resistance. Neurosci Lett 456:25-29.
717 Pérez-Pinzón M, Tao L, Nicholson C (1995) Extracellular potassium, volume fraction, and
718 tortuosity in rat hippocampal CA1, CA3, and cortical slices during ischemia. J
719 Neurophysiol 74:565-573.

720 Prinz AA, Bucher D, Marder E (2004) Similar network activity from disparate circuit parameters.
721 Nat Neurosci 7:1345-1352.
722 Ransdell JL, Nair SS, Schulz DJ (2012) Rapid homeostatic plasticity of intrinsic excitability in a
723 central pattern generator network stabilizes functional neural network output. J
724 Neurosci 32:9649-9658.
725 Rodgers CI, Armstrong GA, Shoemaker KL, LaBrie JD, Moyes CD, Robertson RM (2007) Stress
726 preconditioning of spreading depression in the locust CNS. PLoS One 2:e1366.
727 Rodgers EW, Krenz W-D, Jiang X, Li L, Baro DJ (2013) Dopaminergic tone regulates transient
728 potassium current maximal conductance through a translational mechanism requiring
729 D1Rs, cAMP/PKA, Erk and mTOR. BMC Neurosci 14:143.
730 Roffman RC, Norris BJ, Calabrese RL (2011) Animal-to-animal variability of connection strength
731 in the leech heartbeat central pattern generator. J Neurophysiol 107:1681-1693.
732 Ruangkittisakul A, Panaitescu B, Ballanyi K (2011) K^+ and Ca^{2+} dependence of inspiratory-related
733 rhythm in novel "calibrated" mouse brainstem slices. Respir Physiol Neurobiol 175:37-
734 48.
735 Rybak IA, Molkov YI, Jasinski PE, Shevtsova NA, Smith JC (2014) Rhythmic Bursting in the Pre-
736 Bötzinger Complex. In: Progress in Brain Research, pp 1-23: Elsevier.
737 Schulz DJ, Goaillard J-M, Marder E (2006) Variable channel expression in identified single and
738 electrically coupled neurons in different animals. Nat Neurosci 9:356-362.
739 Schulz DJ, Goaillard JM, Marder EE (2007) Quantitative expression profiling of identified
740 neurons reveals cell-specific constraints on highly variable levels of gene expression.
741 Proc Natl Acad Sci USA 104:13187-13191.

742 Selverston A, Moulins M (1987) Comparison with other systems. In: The Crustacean
743 Stomatogastric System, pp 307-313. Berlin: Springer.
744 Selverston AI (1976) Neuronal mechanisms for rhythmic motor pattern generation in a simple
745 system. In: Neural control of locomotion, pp 377-399. Boston, MA: Springer.
746 Selverston AI, Miller JP (1980) Mechanisms underlying pattern generation in lobster
747 stomatogastric ganglion as determined by selective inactivation of identified neurons. I.
748 Pyloric system. J Neurophysiol 44:1102-1121.
749 Selverston AI, Miller JP, Wadepuhl M (1982) Local circuits for the generation of rhythmic motor
750 patterns. Journal de Physiologie 78:748-754.
751 Sharma N, Gabel Harrison W, Greenberg Michael E (2015) A Shortcut to Activity-Dependent
752 Transcription. Cell 161:1496-1498.
753 Shruti S, Schulz DJ, Lett KM, Marder E (2014) Electrical coupling and innexin expression in the
754 stomatogastric ganglion of the crab Cancer borealis. J Neurophysiol 112:2946-2958.
755 Silver IA, Erecinska M (1994) Extracellular glucose concentration in mammalian brain:
756 continuous monitoring of changes during increased neuronal activity and upon
757 limitation in oxygen supply in normo-, hypo-, and hyperglycemic animals. J Neurosci
758 14:5068-5076.
759 Somjen GG (1979) Extracellular potassium in the mammalian central nervous system. Ann Rev
760 Physiol 41:159-177.
761 Somjen GG (2001) Mechanisms of Spreading Depression and Hypoxic Spreading Depression-
762 Like Depolarization. Physiol Rev 81:1065-1096.

763 Somjen GG (2002) Ion Regulation in the Brain: Implications for Pathophysiology. The
764 Neuroscientist 8:14.
765 Soofi W, Goeritz ML, Kispersky TJ, Prinz AA, Marder E, Stein W (2014) Phase maintenance in a
766 rhythmic motor pattern during temperature changes *in vivo*. J Neurophysiol 111:2603-
767 2613.
768 Stein W, DeLong ND, Wood DE, Nusbaum MP (2007) Divergent co-transmitter actions underlie
769 motor pattern activation by a modulatory projection neuron. Eur J Neurosci 26:1148-
770 1165.
771 Swensen AM, Bean BP (2005) Robustness of burst firing in dissociated Purkinje neurons with
772 acute or long-term reductions in sodium conductance. J Neurosci 25:3509-3520.
773 Tang LS, Taylor AL, Rinberg A, Marder E (2012) Robustness of a rhythmic circuit to short- and
774 long-term temperature changes. J Neurosci 32:10075-10085.
775 Tang LS, Goeritz ML, Caplan JS, Taylor AL, Fisek M, Marder E (2010) Precise temperature
776 compensation of phase in a rhythmic motor pattern. PLoS Biol 8:e1000469.
777 Taylor AL, Goaillard J-M, Marder E (2009) How multiple conductances determine
778 electrophysiological properties in a multicompartment model. J Neurosci 29:5573-5586.
779 Temporal S, Lett KM, Schulz DJ (2014) Activity-dependent feedback regulates correlated ion
780 channel mRNA levels in single identified motor neurons. Curr Biol 24:1899-1904.
781 Thoby-Brisson M, Simmers J (1998) Neuromodulatory inputs maintain expression of a lobster
782 motor pattern-generating network in a modulation-dependent state: evidence from
783 long-term decentralization in vitro. J Neurosci 18:2212-2225.

784 Thoby-Brisson M, Simmers J (2002) Long-Term Neuromodulatory Regulation of a Motor
785 Pattern–Generating Network: Maintenance of Synaptic Efficacy and Oscillatory
786 Properties. J Neurophysiol 88:2942-2953.
787 Tornqvist K, Yang X, Dowling J (1988) Modulation of cone horizontal cell activity in the teleost
788 fish retina. III. Effects of prolonged darkness and dopamine on electrical coupling
789 between horizontal cells. J Neurosci 8:2279-2288.
790 Tran T, Unal CT, Severin D, Zaborszky L, Rotstein HG, Kirkwood A, Golowasch J (2019) Ionic
791 current correlations are ubiquitous across phyla. Sci Rep 9:1687.
792 Turrigiano G (2012) Homeostatic synaptic plasticity: local and global mechanisms for stabilizing
793 neuronal function. Cold Spring Harb Perspect Biol 4:a005736.
794 Von Euler C (1983) On the central pattern generator for the basic breathing rhythmicity. J Appl
795 Physiol 55:1647-1659.
796 Wood DE, Stein W, Nusbaum MP (2000) Projection neurons with shared cotransmitters elicit
797 different motor patterns from the same neural circuit. J Neurosci 20:8943-8953.
798
799

800 FIGURE LEGENDS

801

802 **Figure 1. The pyloric rhythm is disrupted by large changes in extracellular**
803 **[K^+].** The pyloric rhythm remains robust when exposed to 1.5x[K^+] saline and is
804 disrupted at higher [K^+]. (A) Diagram of the dissected stomatogastric nervous system
805 (STNS). The entire STNS was superfused with saline with altered [K^+]. (B) The triphasic
806 pyloric rhythm is illustrated in an extracellular recording from *lvn,* which contains
807 axons from LP, PY and PD neurons. (C) Connectivity diagram of the pyloric circuit of
808 the crab *Cancer borealis*. (D - G) *lvn* recordings of spiking activity during application of
809 elevated [K^+] saline (green boxes) in concentrations of 1.5x, 2.0x, 2,5x and 3.0x the
810 physiological concentration of potassium.

811

812 **Figure 2. Representative activity of pyloric circuit neurons, pyloric dilator**
813 **(PD) and lateral pyloric (LP) neurons 2.5x[K^+] saline.** Green shaded boxes
814 indicate the period of 2.5x[K^+] saline superfusion. (A) 3-second segments of PD and LP
815 activity (i-v) are shown in physiological saline, 10, 20 and 70 min into application of
816 2.5x[K^+] saline and upon return to physiological saline. (B) Voltage trace of a PD
817 neuron's activity for the entire representative experiment. (C) Interspike intervals of the
818 PD neuron's activity over the course of 2.5x[K^+] saline application. ISIs are plotted on a
819 log scale, with the presence of only one band indicating a tonic firing regime and two
820 bands indicating bursting activity. (D) Spectrogram of the PD neuron's voltage trace.
821 The color code in each spectrogram represents the amplitude density. (E) Mean
822 minimum membrane potential of all PD neurons in five-minute bins for each
823 preparation. (F) Average change in PD neurons' minimum membrane potential

824 compared to baseline in five-minute bins for all preparations. Error bars represent
825 standard deviations. Minimum membrane potential increased significantly when
826 2.5x[K^+] saline was applied (repeated measures ANOVA, Tukey post-hoc $p<0.05$), but
827 did not change significantly between 10 and 90 minutes in 2.5x[K^+] (n.s., all $p > 0.05$).
828 The PD minimum membrane potential returned to baseline levels in wash of
829 physiological saline (n.s., baseline compared to wash, all $p > 0.05$).
830
831 **Figure 3. Responses to 2.5x[K^+] saline are highly variable across**
832 **preparations.** Shaded green boxes indicate the period of 2.5x[K^+] saline superfusion**.**
833 Example traces of PD neurons from four different preparations (A-D) with a
834 characteristic crash and recovery of activity in 2.5x[K^+] saline are shown along with the
835 corresponding log(ISIs) for each preparation. (E) Time to recovery of activity in PD
836 neurons is not correlated to the baseline minimum membrane potential ($R^2 = 0.203$),
837 (F) the change in minimum membrane potential when 2.5x[K^+] is applied ($R^2 = 0.104$),
838 or (G) the burst frequency of the PD neuron at baseline conditions ($R^2 = 0.012$).
839
840 **Figure 4. The representative activity of a PD neuron with presynaptic**
841 **glutamatergic synapses blocked with picrotoxin (PTX) in 2.5x[K^+] saline.**
842 (A) Connectivity diagram of the pyloric network with picrotoxin (PTX) blocking
843 glutamatergic signaling. (B) 3-second segments of PD activity (i-vi) in physiological
844 saline, 20 min into application of 10^{-5}M PTX saline, and at 10, 20 and 70 min into
845 application of 2.5x[K^+] PTX saline and upon return to physiological saline (C). Voltage
846 trace of the PD neuron over the entire experiment. The blue shaded boxes indicate time
847 of 10^{-5}M PTX saline superfusion, and the green shaded box indicates the 90-minute

848 period of 2.5x[K^+] PTX saline superfusion. This color scheme is maintained D, F, and G.
849 (D) ISIs over the course of the experiment plotted on a log scale, with the presence of
850 one band indicating a tonic firing regime and two bands indicating bursting activity. (E)
851 Spectrogram of PD neuron's voltage trace. The color code reflects the amplitude density.
852 (F) Mean minimum membrane potential of all PTX(+) PD neurons in five-minute bins
853 for each preparation. (G) Average change in PD neurons' minimum membrane potential
854 in five-minute bins compared to baseline for all preparations. Error bars represent
855 standard deviations. Minimum membrane potential increases significantly when
856 2.5x[K^+] PTX saline is applied (repeated measures ANOVA, Tukey post-hoc comparing
857 baseline to 2.5x[K^+], all $p<0.05$) but does not change significantly after 10 minutes in
858 2.5x[K^+] PTX for the duration of the elevated [K^+] application (n.s., all $p > 0.05$). The
859 minimum membrane potential returned to baseline levels in wash of physiological
860 saline (n.s., baseline compared to wash, all $p > 0.05$).
861
862 **Figure 5. PD neurons respond differently to 2.5x[K^+] saline in the presence**
863 **and absence of PTX.** (A) Activity patterns of PD neurons in control conditions
864 exposed to 2.5x[K^+] saline. (B) Activity patterns of PTX(+)PD neurons exposed to
865 2.5x[K^+] PTX saline. (C) Control PD neurons exhibit a longer period of silence upon
866 2.5x[K^+] saline application compared to PD neurons in PTX (Wilcoxon rank-sum test p
867 = 0.0129). (D) Control PD neurons exhibit a longer period of sparse firing upon 2.5x[K^+]
868 saline application compared to PD neurons in PTX (Wilcoxon rank-sum test p = 0.034).
869 (E) Control PD neurons do not show significant differences in the amount of time in
870 tonic firing (n.s., p = 0.77) or in (F) burst firing upon 2.5x[K^+] saline application
871 compared to PD neurons in PTX (n.s., p = 0.51).

872

873 **Figure 6. Action potential thresholds rapidly change in PD neurons during**
874 **exposure to 2.5x[K^+].** (A) Two-electrode current clamp was used to inject current
875 ramps from -4nA to +2nA over 60 seconds. Representative activity during ramps from a
876 PD neuron in 2.5x[K^+] at 5, 10, 40, and 80 minutes after the onset of 2.5x[K^+] saline
877 application. (B) From the representative neuron shown in A, for each ramp in 2.5x[K^+]
878 saline, the average firing frequencies in 5-second bins are plotted against the average
879 membrane potential of the corresponding bin. For C, D and E, green boxes indicate time
880 of 2.5x[K^+] saline superfusion, and blue boxes indicate time of PTX superfusion. (C) PD
881 neuron spike thresholds for each ramp are plotted for each preparation (different
882 colors) in the absence of PTX. (D) PD neuron spike thresholds for each ramp plotted for
883 each preparation in PTX. (E) Percent change in the spike threshold over the course of
884 the experiment (as compared to the last baseline ramp) for PD neurons in the presence
885 and absence of PTX. Error bars are SEM, one-way ANOVA with Tukey Post-Hoc test (*
886 = $p < 0.05$, all comparisons between brackets). (F) Average F-I curves for PD neurons
887 (solid lines) and PD neurons in PTX (dashed lines) at five minutes after the onset of
888 2.5x[K^+] saline application (purple lines) and at 90 minutes after the onset of 2.5x[K^+]
889 saline application (red lines). There was a significant difference between the F-I curve
890 for control PD neurons between the 5- and 90-minute time points (Two-way repeated
891 measures ANOVA, $p = 0.009$). In addition, there was a significant difference in the F-I
892 curves of PTX(+) and PTX(-) PD neurons after 5 minutes in 2.5x[K^+] saline (Two-way
893 repeated measures ANOVA, $p = 0.036$).

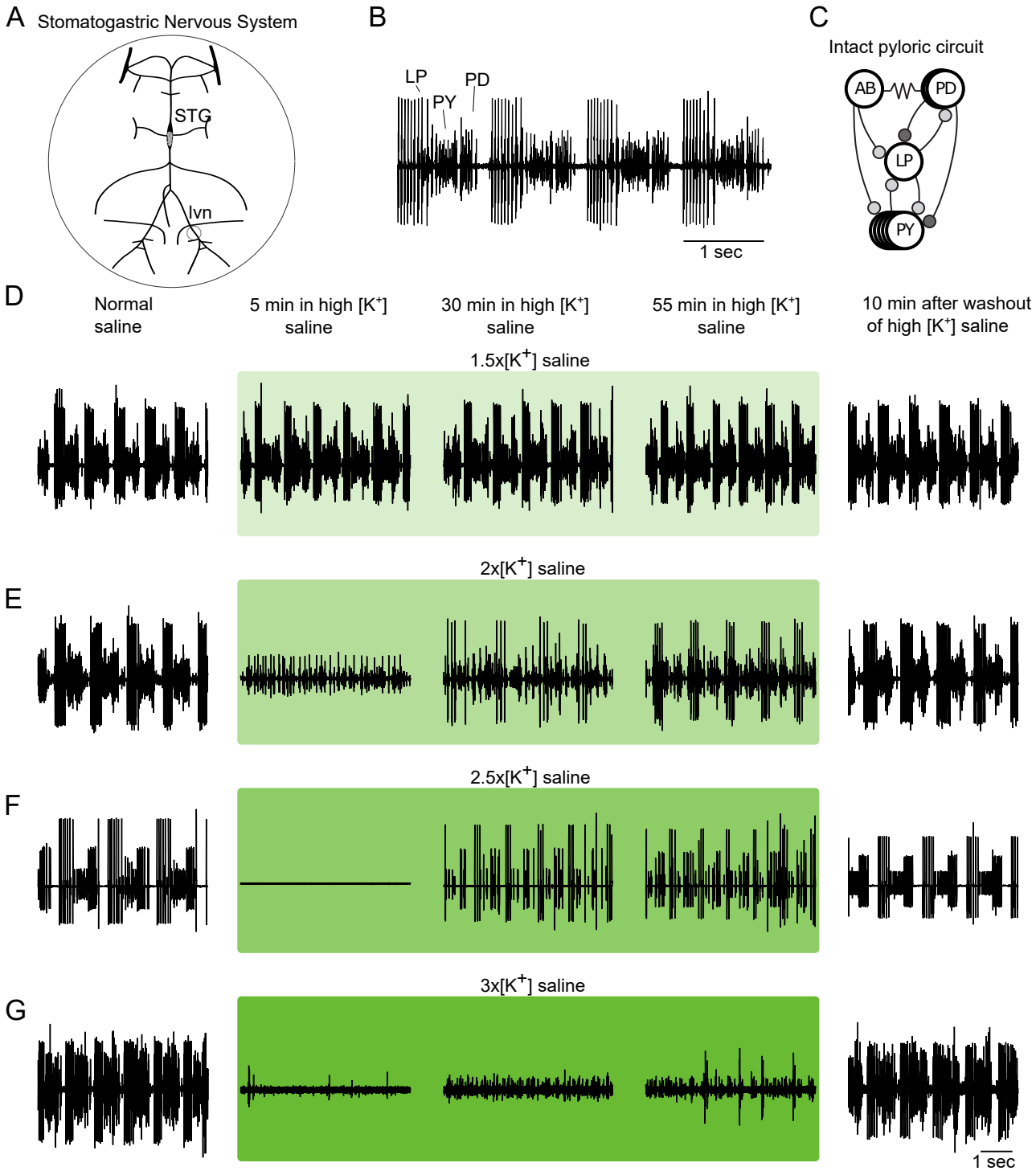
A
Stomatogastric Nervous System
STG
lvn
B
LP
PD
PY
1 sec
C
Intact pyloric circuit
AB
PD
LP
PY
D
Normal saline
5 min in high [K+] saline
30 min in high [K+] saline
55 min in high [K+] saline
10 min after washout of high [K+] saline
1.5x[K+] saline
E
2x[K+] saline
F
2.5x[K+] saline
G
3x[K+] saline
1 sec

Figure 1

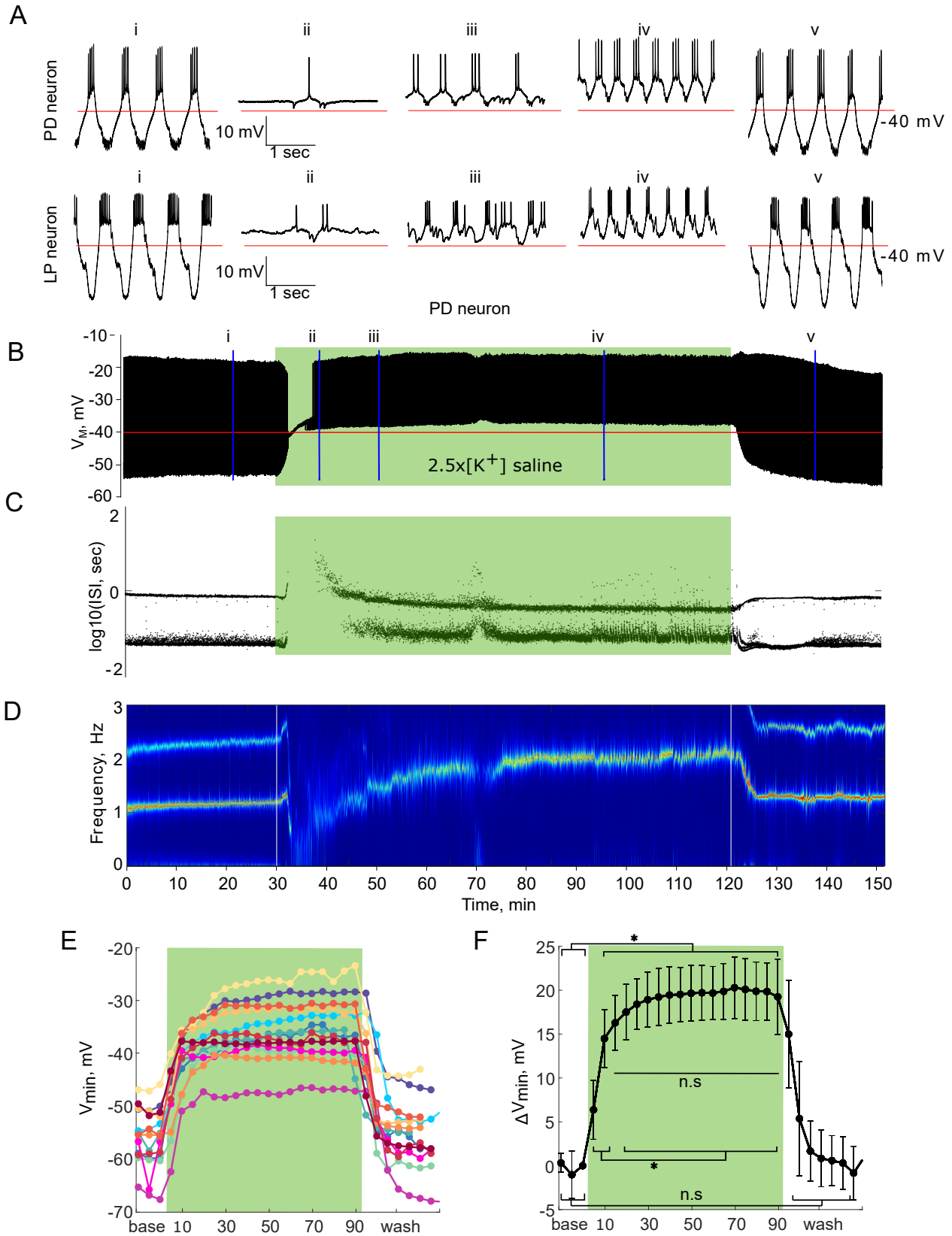
A
i
ii
iii
iv
v
PD neuron
10 mV
1 sec
-40 mV
LP neuron
PD neuron
B
V_M, mV
2.5x[K^+] saline
C
log10(ISI, sec)
D
Frequency, Hz
Time, min
E
V_{min}, mV
base
wash
F
ΔV_{min}, mV
n.s
*

Figure 2

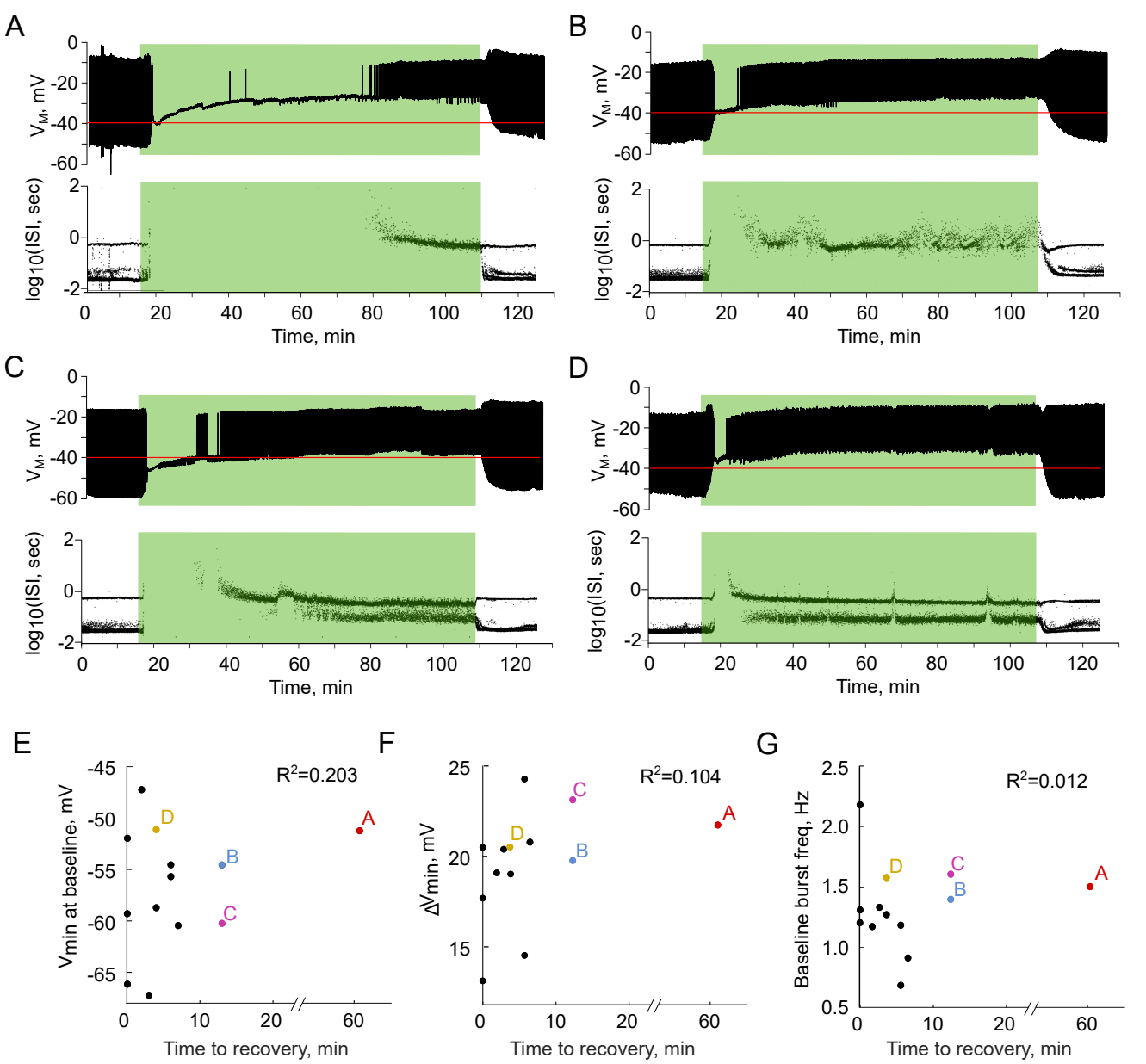
A
B
C
D
V_M, mV
log10(ISI, sec)
Time, min

E
F
G
R^2=0.203
R^2=0.104
R^2=0.012
Vmin at baseline, mV
ΔVmin, mV
Baseline burst freq, Hz
Time to recovery, min
A
B
C
D

Figure 3

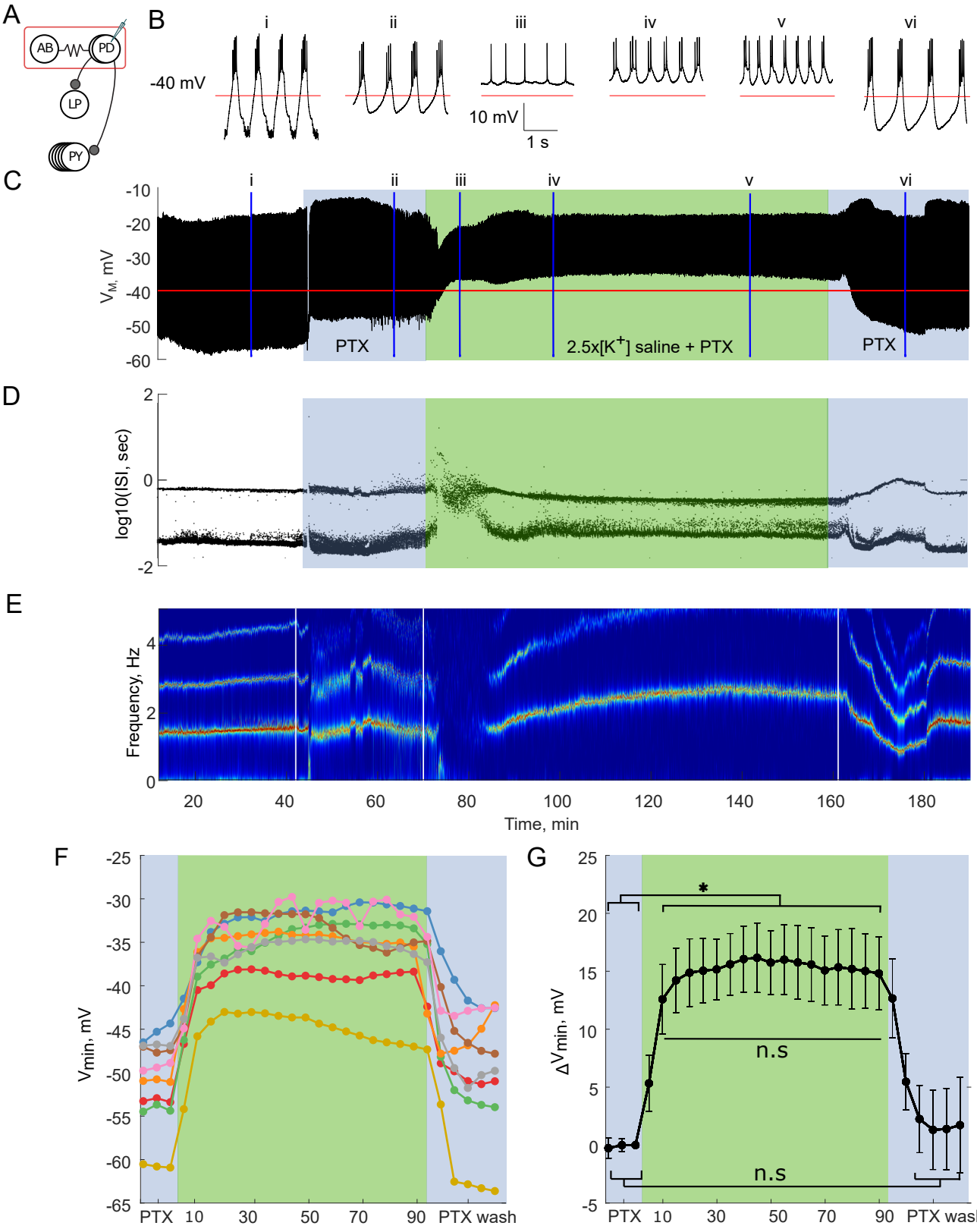
A
AB
PD
LP
PY
B
-40 mV
i
ii
iii
iv
v
vi
10 mV
1 s
C
i
ii
iii
iv
v
vi
-10
-20
-30
-40
-50
-60
V_M, mV
PTX
2.5x[K+] saline + PTX
PTX
D
2
0
-2
log10(ISI, sec)
E
4
2
0
Frequency, Hz
20
40
60
80
100
120
140
160
180
Time, min
F
-25
-30
-35
-40
-45
-50
-55
-60
-65
Vmin, mV
PTX
10
30
50
70
90
PTX wash
G
25
20
15
10
5
0
-5
ΔVmin, mV
*
n.s
n.s
PTX
10
30
50
70
90
PTX wash

Figure 4

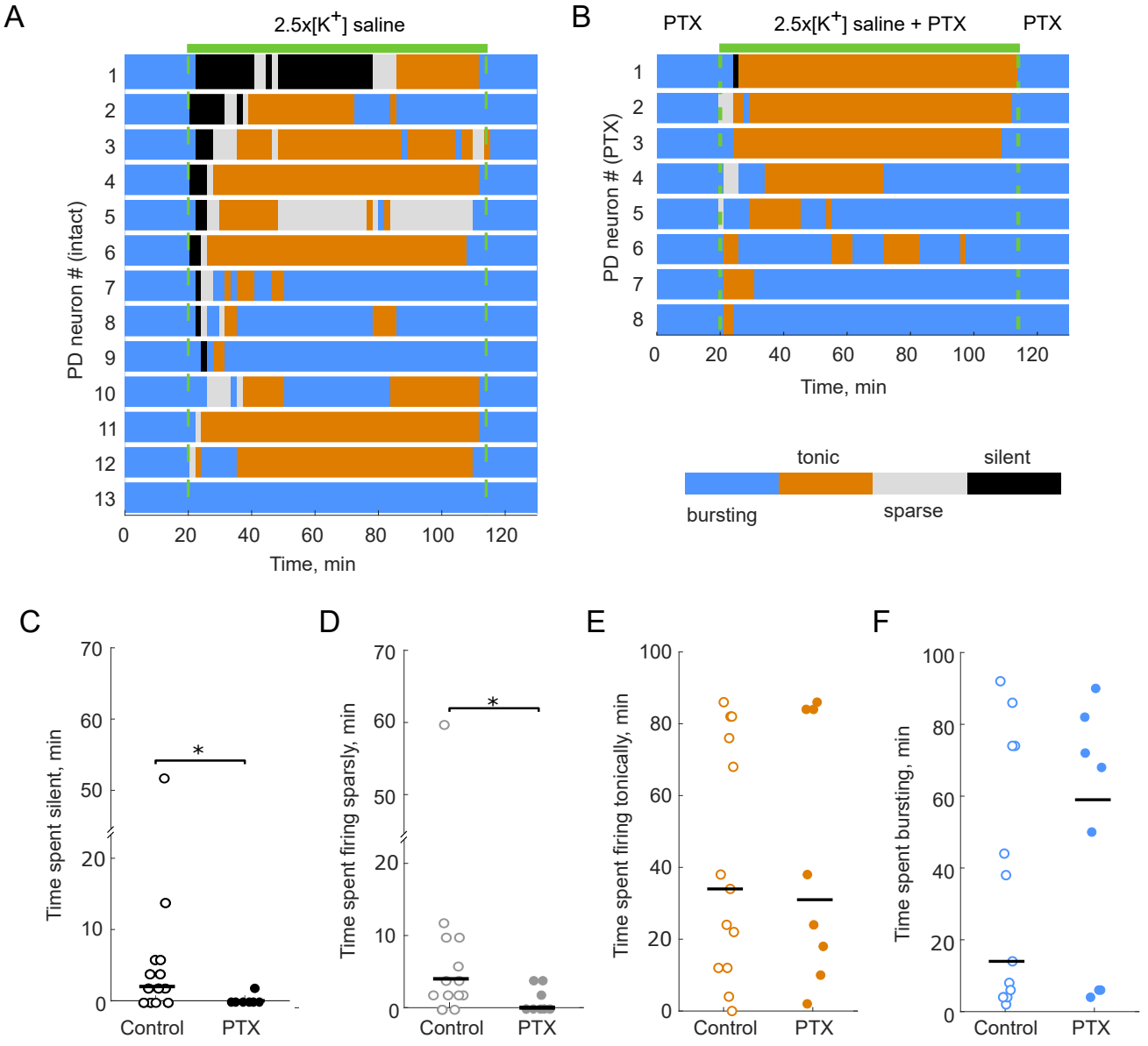
A
2.5x[K+] saline
PD neuron # (intact)
Time, min
B
PTX
2.5x[K+] saline + PTX
PTX
PD neuron # (PTX)
Time, min
tonic
silent
bursting
sparse
C
Time spent silent, min
Control
PTX
D
Time spent firing sparsly, min
Control
PTX
E
Time spent firing tonically, min
Control
PTX
F
Time spent bursting, min
Control
PTX

Figure 5

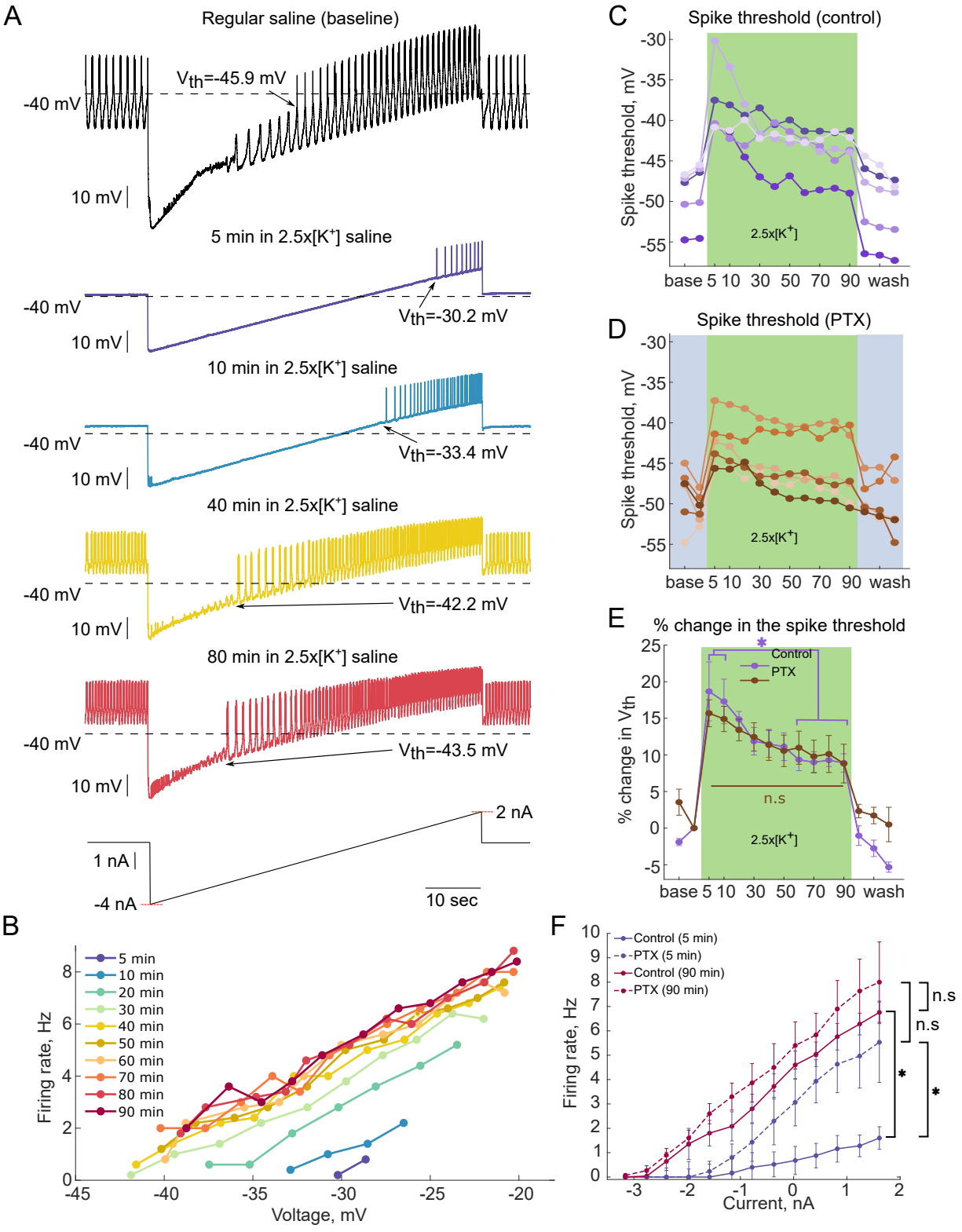
A
Regular saline (baseline)
Vth=-45.9 mV
-40 mV
10 mV
5 min in 2.5x[K+] saline
Vth=-30.2 mV
10 min in 2.5x[K+] saline
Vth=-33.4 mV
40 min in 2.5x[K+] saline
Vth=-42.2 mV
80 min in 2.5x[K+] saline
Vth=-43.5 mV
2 nA
1 nA
-4 nA
10 sec
C
Spike threshold (control)
Spike threshold, mV
2.5x[K+]
base 5 10 30 50 70 90 wash
D
Spike threshold (PTX)
E
% change in the spike threshold
Control
PTX
% change in Vth
n.s
B
5 min
10 min
20 min
30 min
40 min
50 min
60 min
70 min
80 min
90 min
Firing rate, Hz
Voltage, mV
F
Control (5 min)
PTX (5 min)
Control (90 min)
PTX (90 min)
Current, nA

Figure 6